Natural Resources Canada | Ressources naturelles Canada

# Targeted Geoscience Initiative 4: Increasing Deep Exploration Effectiveness

## Sulfide Paragenesis and LA-ICP-MS Arsenopyrite Geochemistry at the Meliadine Gold District, Nunavut: Implications for Re-Os Arsenopyrite Geochronology and Ore Deposit Genesis


Christopher Lawley[1]*, Benoît Dubé[2], Simon Jackson[1], Zhaoping Yang[1], Patrick Mercier-Langevin[2], and Denis Vaillancourt[3]
[1]Natural Resources Canada, Geological Survey of Canada, 601 Booth Street, Ottawa, K1A 0E8, Canada
[2]Ressources naturelles Canada, Commission géologique du Canada, 490 rue de la Couronne, Québec, G1K 9A9, Canada
[3]Agnico-Eagle Mines Limited, 765 chemin de la Mine Goldex, Val D'Or, Québec, J9P 4N9, Canada
*clawley@NRCan.gc.ca; (613) 996 2593



OPEN FILE 7491 — Contributions to this publication do not necessarily reflect the views or policies of Natural Resources Canada. For permission to reproduce or translate all or any part of this publication, contact Public Information Services, 580 Booth Street, 4th floor, Ottawa, Ontario K1A 0E8. 2014

© Her Majesty the Queen in Right of Canada 2014
doi:10.4095/293958
This publication is available for free download through GEOSCAN
(http://geoscan.nrcan.gc.ca/).

Recommended citation
Lawley, C.J.M., Dubé, B., Jackson, S., Yang, Z., Mercier-Langevin, P., Vaillancourt, D., 2014, Sulfide paragenesis and LA-ICP-MS arsenopyrite geochemistry at the Meliadine Gold District, Nunavut: implications for Re-Os arsenopyrite geochronology and ore deposit genesis; Geological Survey of Canada, Open File 7491, 1 poster, doi:10.4095/293958


Geological Survey of Canada with Provincial and Territorial Collaboration

## 1. Introduction

The genesis of Banded Iron Formation (BIF)-hosted gold deposits in the Western Churchill Province, Nunavut, remain poorly understood (Fig. 1). The age of these deposits is particularly unclear, although previous geochronology studies have suggested that gold was introduced during Paleoproterozoic re-working of Archean BIFs (e.g., Meliadine, Carpenter et al., 2005; and Three Bluffs, Davies et al., 2011 ). However, the absolute timing of gold deposition can remain equivocal in the absence of a robust paragenetic framework due to the reliance on mineral proxies for geochronology and the difficulty in directly dating gold. In this contribution, we report new petrographic and SEM results which, together with Laser Ablation-Inductively Coupled Plasma-Mass Spectrometry (LA-ICP-MS) arsenopyrite geochemistry, provide new constraints on sulfide paragenesis at the Tiriganiaq deposit, Meliadine gold district, Nunavut (Fig. 2). These results form the foundation of an on-going Re-Os arsenopyrite geochronology study and broader TGI-4 investigation into the geologic setting of several gold deposits within the Meliadine gold district.

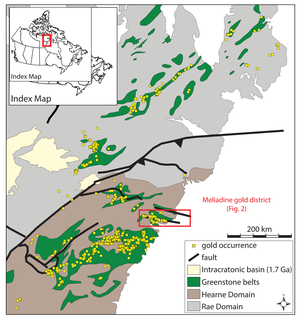


*Figure 1 - Regional geology map showing the location of the Meliadine gold district and other gold occurrences in the Western Churchill Province (modified from Davis et al., 2006).*

## 2. Local geology

The Agnico-Eagle Meliadine project contains an estimated 3 Moz of gold in proven and probable reserves (13.3 Mt at 7.0 g/t) within a larger mineral resource (www.agnicoeagle.com). The majority of gold deposits within the Meliadine gold district are spatially associated with the Pyke fault, which is a ≥80 km long structure that cuts Archean (ca. 2.66 Ga; Tella et al., 1995) greenschist-amphibolite facies igneous and supracrustal rocks packages of the Rankin Inlet Group (Fig. 2). Tiriganiaq is the largest of the currently explored deposits and is primarily hosted by BIF and associated with an E-W trending and steeply north-dipping splay of the Pyke fault (Fig. 2).

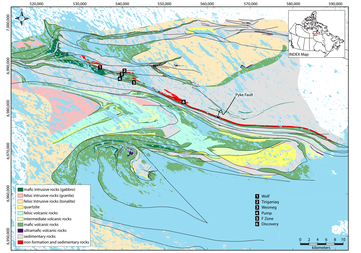


*Figure 2 - Local geology map for the Meliadine gold district (courtesy of Agnico-Eagle Mines). Map shows the location of the Tiriganiaq deposit and the trace of the Pyke fault.*

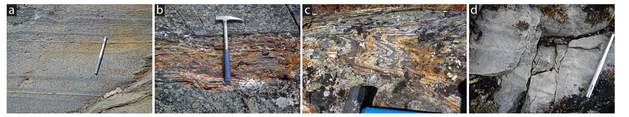

*Figure 3 - field photos: (a) greywacke with biotite porphyroblasts; (b) narrow BIF horizon interbedded with volcaniclastics; (c) mineralized BIF at Discovery; and (d) quartzite near Discovery and adjacent to the Pyke fault.*


**Acknowledgements and References**

The authors would like to thank Agnico-Eagle Mines for access to exploration drill core.



Cabri, L., Jackson, S., 2011. New developments in characterization of sulphide refractory Au ores: "World Gold 2011" Conference of Metallurgists, Montréal, QC, October, 2011: Proceedings of the 50th Conference of Metallurgists, 51-62.

Carpenter, R.L., Duke, N.A., Sandeman, H.A., Stern, R., 2005. Relative and absolute timing of gold mineralization along the Meliadine trend, Nunavut, Canada: Evidence for Paleoproterozoic gold hosted in an Archean greenstone belt. Economic Geology, 100, 567-576.

Davies, T., Richards, J.P., Hearman, J.M., Chacko, T., Simonetti, A., Williamson, J., McDonald, D.W., 2012. Paleoproterozoic age relationships in the Three Bluffs Archean Gold Deposit, Committee Bay Greenstone Belt, Nunavut, Canada: Exploration and Mining Geology, 19, 33-80.

Davis, W.J., Hanmer, S., Tella, S., Dandenman, H.A., Ryan, J.J., 2006. U-Pb geochronology of the MacQuoid supracrustal belt and Cross Bay plutonic complex: Key components of the northwestern Hearne subdomain, western Churchill Province, Nunavut, Canada: Precambrian Research, 145, 53-80.

Griffin, W.L., Powell, W.J., Pearson, N.J., O'Reilly, S.Y., 2008. GLITTER: Data reduction software for laser ablation ICP–MS, in: Laser Ablation-ICP-Mass Spectrometry in the Earth Sciences: Current Practices and Outstanding Issues (Sylvester, P., Ed.). Mineralogical Association of Canada (MAC) Short Course Series, 40, 308-311.

R Development Core Team, 2008. R: A language and environment for statistical computing. R Foundation for Statistical Computing, Vienna, Austria. ISBN 3-900051-07-0, URL http://www.R-project.org.

Reich, M., Kesler, S.E., Utsunomiya, S., Palenik, C.S., Chryssoulis, S.L., Ewing, R.C., 2005. Solubility of gold in arsenian pyrite. Geochimica et Cosmochimica Acta, 69, 2781–2796.

Tella, S., Roddick, J.C., van Breemen, O., 1995. U-Pb zircon age for a volcanic suite in the Rankin Inlet Group, Rankin Inlet map area, District of Keewatin, Northwest Territories. Geologic Survey of Canada, Radiogenic Age and Isotopic Studies Report 9, 11-15.


## 3. Core photos

Gold occurs in a variety of host rocks at the Meliadine gold district, but is primarily hosted by hydrothermally altered BIF (Fig. 4) and quartz veins (Figs. 4c, d) at the Tiriganiaq deposit (Fig. 2). Archean host rocks are cut by Paleoproterozoic (ca. 1.85 Ga; Carpenter et al., 2005) quartz (± carbonate) veins and lamprophyre dikes (Fig. 4f), which suggests that gold was introduced during Paleoproterozoic re-working of Archean rocks. However, the potential for Archean gold metallogeny and the prospectivity of Archean structures for gold remains poorly understood.

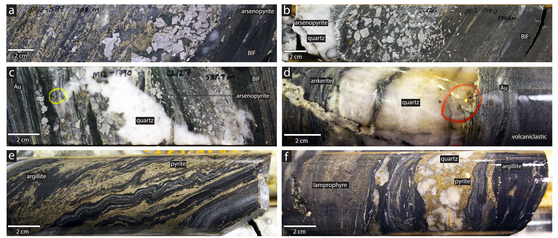


*Figure 4 - Core photos: (a) sulfidized BIF from ore zone at Tiriganiaq. Coarse grained and idioblastic arsenopyrite are generally associated with high gold grades, however arsenopyrite contains relatively low refractory gold concentrations (Fig. 7); (b) arsenopyrite concentrated adjacent to quartz vein cutting sulphidized BIF; (c) quartz vein with visible gold cutting BIF; (d) coarse grained gold at quartz vein margin cutting volcaniclastic host rocks; (e) gold-bearing and sulphidized argillite at Tiriganiaq ; (f) lamprophyre dikes cut sulphidized and argillite in the main ore zone. The timing of the dikes is unclear, but if related to the Christopher Island Formation could suggest that gold is >1.83 Ga.*

## 4. Petrography

At Tiriganiaq, gold is primarily associated with arsenopyrite ± pyrrhotite ± pyrite ± chalcopyrite ± galena bearing altered BIF and quartz veins (Figs. 5, 6). Gold occurs as inclusions within coarse grained and idioblastic arsenopyrite (Figs. 5a, b, e, f), but also occurs as arsenopyrite fracture fills along with pyrrhotite ± pyrite and lesser amounts of galena ± chalcopyrite (Figs. 5a–d, h, 6a–d).

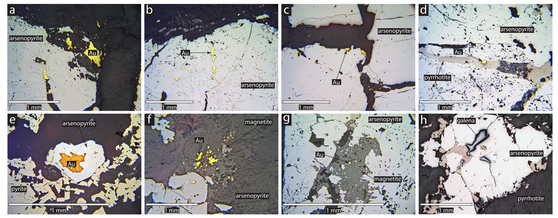


*Figure 5 - Reflected light photomicrographs: (a) gold inclusions within arsenopyrite and disseminated within quartz-carbonate vein; (b) gold inclusions and gold filling arsenopyrite fractures; (c) gold concentrated along arsenopyrite grain boundaries and filling arsenopyrite fractures; (d) gold and pyrhotite associated with arsenopyrite fractures; (e) coarse grained gold inclusions within arsenopyrite; (f) gold occurs as inclusions within arsenopyrite and magnetite; (g) gold inclusions within magnetite; (h) galena and pyrrhotite filling arsenopyrite fractures.*

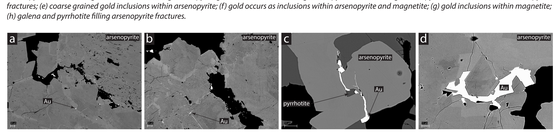


*Figure 6 - SEM BSE images: (a–b) Subtle arsenopyrite zonation/alteration. These arsenopyrite domains can also be distinguished by their trace element composition (Figs. 11 , 12). Gold appears concentrated along fractures; (c) gold and pyrrhotite filling arsenopyrite fracture; (d) gold filling arsenopyrite fracture. Note subtle arsenopyrite zoning.*

## 5. LA-ICP-MS spot analyses

LA-ICP-MS analyses were conducted at the Geological Survey of Canada using an Agilent Techonologies 7700x ICP-MS coupled to a Photon Machines Analyte 193 nm excimer laser ablation system (Cabri and Jackson, 2011). Laser operating conditions (5.71 J/cm$^2$ fluence, 10 Hz repetition rate, 43 µm spot size) were used for standard (GSE-1G, MASS-1, and doped synthetic pyrrhotite Po689)-sample-standard bracketing. Iron content was used as an internal standard to correct for different ablation yield between sample and calibration standards. This approach also corrects, to some extent, for matrix effects and signal drift in the ICP-MS. The element suite (Ag, Bi, Cd, Co, Cr, Cu, Hg, In, Mo, Ni, Pb, Pd, Pt, Re, Sb, Se, Sn, Te, W) was determined during 60s of sample ablation preceded by 40 s of gas background. Data reduction was completed using GLITTER (Griffin et al., 2008). Arsenopyrite spot analyses from five ore zone samples collected at the Tiriganiaq deposit are shown below (Fig. 7).

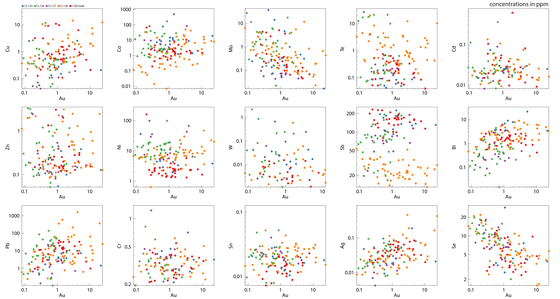


*Figure 7 - Log-log scatter plots showing selected trace element concentrations plotted against gold (concentrations not transformed or imputed; see below). Note the significant geochemical overlap between samples and the relatively low refractory gold concentration (i.e., <23 ppm; well below the solubility of gold within arsenopyrite; Reich et al., 2005) of for all five of the studied samples. All concentrations are reported in ppm.*

The majority of trace element concentration distributions are non-normal (i.e., right skewed with positive outliers) and some analyses were below the detection limit of the method. In figures 8–9, these 'missing values' are replaced following the Nearest Neighbour approach and the data set is transformed (Centered Log Ratio Transformation; CLR) in order to obtain a more normal distribution and to reduce the influence of outlying values (data manipulation was completed using R software and the R packages 'composition' and 'robCompositions'; R Development Team, 2008). Despite the broad inter- and intra-sample geochemical overlap, some arsenopyrite samples possess geochemically distinct signatures (e.g., Sb, Ni; Figs. 8a, 9). Each of the five ore zone arsenopyrite samples share a similar paragenesis and thus these unique geochemical signatures may be related to fracture-controlled trace element heterogeneity at the crystal scale (Figs. 11, 12).

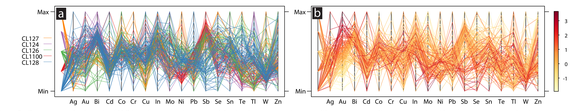


*Figure 8 - Parallel coordinate plots of CLR transformed data summarizing the trace element composition of arsenopyrite samples: (a) plot is colour coded according to sample number and shows broad geochemical overlap between samples, but also shows diverging patterns for some trace elements (e.g., Bi, Cu, Ni, and Sb); (b) plot is colour coded to gold concentration and shows broad compositional overlap between analyses with high and low refractory gold concentrations. However, the highest refractory gold concentrations are relatively enriched in Bi and generally depleted in Sb, Se and Mo (most pronounced for CL128). Similar antithetic relationships between Au and Sb-Mo are also observed in element maps (Fig. 11j, m, p).*

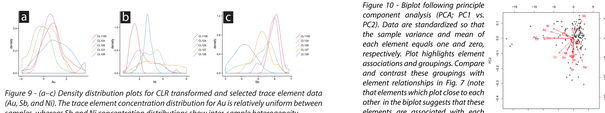


*Figure 9 – (a–c) Density distribution plots for CLR transformed and selected trace element data (Au, Sb, and Ni). The trace element concentration distribution for Au is relatively uniform between samples, whereas Sb and Ni concentration distributions show inter-sample heterogeneity*

*Figure 10 - Biplot following principle component analysis (PCA; PC1 vs. PC2). Data are standardized so that the sample variance and mean of each element equals one and zero, respectively. Plot highlights element associations and groupings. Compare and contrast these groupings with element relationships in Fig. 7 (note that elements which plot close to each other in the biplot suggests that these elements are associated with each other)*

## 6. LA-ICP-MS in situ 'element mapping'

In situ 'element mapping' was performed using a grid sampling pattern comprising thousands of individual 10 µm spot analyses following the approach of Cabri and Jackson (2011). Selected element concentration maps (Figs. 11, 12), reported in log scale, show geochemically distinct domains within individual arsenopyrite crystals. These domains appear to be fracture-controlled and suggest arsenopyrite deformation and re-crystallization were coupled with trace element enrichment. The effects of the latter on Re-Os systematics remains unclear since Re concentrations were generally below detection (Fig. 11r).




*Figure 11 - (a) Thin section scan of mapping sample; (b) reflected light photomicrograph of arsenopyrite crystal. Red box shows approximate limits of the 'element map'; (c) sketch map of arsenopyrite crystal highlighting fractures and small mineral inclusions within the mapped arsenopyrite crystal. Compare and contrast the sketch map with the trace element compositions below (Fig. 11d–r).*

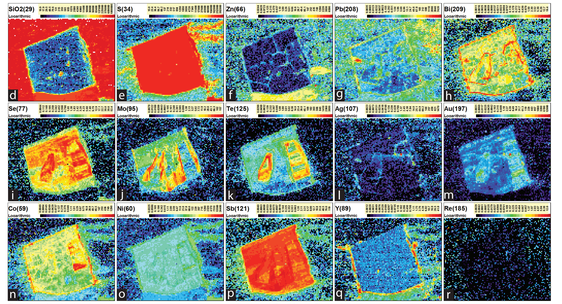


*Fig. 11 cont'd - (d–r) major and trace element maps of the arsenopyrite crystal (Fig. 10a–c). Figure shows how the trace element distribution appears to be, in part, fracture-controlled. Au, Ag, and Te are relatively enriched in two fracture-controlled domains. Note the antithetic relationship between Mo-Sb and Te-Au.*

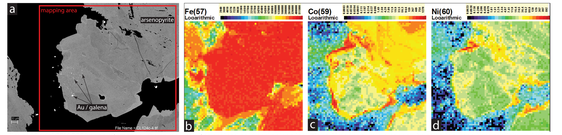


*Figure 12 - (a) SEM BSE image of arsenopyrite crystal with fine grained gold and galena inclusions. Note the subtle arsenopyrite zonation (seen here as slight variation in grey shading); (b–d) selection of major and trace element maps for arsenopyrite crystal (Fig. 12a) showing the geochemical characteristics of arsenopyrite domains. Note that lighter grey areas in Fig. 10a appear relatively enriched in Co and Ni (not shown are similar Se, Pb, Sb and Mo enrichment).*

## 7. Conclusions

Arsenopyrite fractures filled with gold and other sulphide minerals (e.g., galena, chalcopyrite, and pyrrhotite; Fig. 5) suggests that gold may have been mobilized during progressive deformation/metamorphism. Gold mobilization is also evident from LA-ICP-MS arsenopyrite geochemistry results, which suggest that arsenopyrite fracturing and associated hydrothermal fluids appear to be relatively enriched in gold, base- and precious-metals, and other transition elements (Fig. 11).

LA-ICP-MS is a powerful tool for identifying geochemically distinct arsenopyrite crystals, and/or domains within individual arsenopyrite crystals, which are generally grouped in mineral separates prepared for Re-Os analysis.

AGNICO EAGLE

Canada